Supplementary Information

Supplementary Tables

	DD	DDB		DDR	
	raw data	raw data	after correction	raw data	after correction
k_{cat} (s^{-1} per head)	1.5 ± 0.8	12.1 ± 0.7	84.7 ± 12.4	15.3 ± 0.5	113.7 ± 8.1
k_{basal} (s^{-1} per head)	0.06 ± 0.09	2.0 ± 0.1	6.9 ± 1.5	1.4 ± 0.3	8.5 ± 1.0
K_M (μM)	1.9 ± 2.1	1.0 ± 0.1	1.1 ± 0.4	0.7 ± 0.1	0.7 ± 0.2

Supplementary Table 1. MT-stimulated ATPase activity of mammalian dynein/dynactin. ATPase data were collected from three independent experiments (mean ± s.d.) and fit to Michaelis Menten kinetics. Errors represent s.e. from the fit. DDB and DDR raw data were corrected for the fraction of dynein assembled with dynactin and the cargo adaptor (9%, see Methods). DD values have high errors because dynein has very low affinity to MTs in the absence of a cargo adaptor, and its ATPase activity is not saturated by the maximum concentration of tubulin used in the assays (5 μM).

DNA substrate	Sequence (5′⟶3′)
ME-one motor	[p] TGC ATC AGT TG GTC AAT ACT AGG AGC AGA GAT GGC AGG AGT CAG ATG AAC AGA TAG TGG AGG CAG GGT CAG CGC GAG ATC GTC TGC CAT ATC TGA AAT CCT GCT [Cy3 or bio]
ME-two motors	[p] GAC AGT CA TG GTC AAT ACT AGG AGC AGA GAT GGC AGG AGT CAG ATG AAC AGA TAG TGG AGG CAG GGT CAG CGC GAG ATC GTC GA GAA CGC TGC ATC AGT TG GTC AAT ACT AGG AGC AGA GAT GGC AGG AGT CAG ATG AAC AGA TAG TGG AGG CAG GGT CAG CGC GAG ATC GTC TGC CAT ATC TGA AAT CCT GCT [Cy3 or bio]
ME-three motors	[p] TG GTC AAT ACT AGG AGC AGA GAT GGC AGG AGT CAG ATG AAC AGA TAG TGG AGG CAG GGT CAG CGC GAG ATC GTC TGA TGG AGG GAC AGT CA TG GTC AAT ACT AGG AGC AGA GAT GGC AGG AGT CAG ATG AAC AGA TAG TGG AGG CAG GGT CAG CGC GAG ATC GTC GA GAA CGC TGC ATC AGT TG GTC AAT ACT AGG AGC AGA GAT GGC AGG AGT CAG ATG AAC AGA TAG TGG AGG CAG GGT CAG CGC GAG ATC GTC TGC CAT ATC TGA AAT CCT GCT [Cy3 or bio]
M1-S1	[p] TGC ATC AGT TG GTC AAT ACT AGG AGC AGA GAT GGC AGG AGT CAG ATG AAC AGA TAG TGG AGG CAG GGT CAG CGC GAG ATC GTC
M1-tag-Cy3	[p] TGC CAT ATC TGA AAT CCT GCT-Cy3
M1-tag-Bio	[p] TGC CAT ATC TGA AAT CCT GCT-Bio
S1-tag splint	GAT ATG GCA GAC GAT CTC
M2-S1	[p] GAC AGT CA TG GTC AAT ACT AGG AGC AGA GAT GGC AGG AGT CAG ATG AAC AGA TAG TGG AGG CAG GGT CAG CGC GAG ATC GTC GA GAA CGC
S1-2 splint	ACT GAT GCA GCG TTC TC
M3-S1	TG GTC AAT ACT AGG AGC AGA GAT GGC AGG AGT CAG ATG AAC AGA TAG TGG AGG CAG GGT CAG CGC GAG ATC GTC TGA TGG AGG
S2-3 splint	TG ACT GTC CCT CCA TCA
MES1C6	[AmMC6] TG GTC AAT ACT AGG AGC AGA GAT GGC AGG AGT CAG ATG AAC AGA TAG TGG AGG CAG GGT CAG CGC GAG ATC GTC
MES2C6	[AmMC6] AT GAC GAT CTC GCG CTG ACC CTG CCT CCA CTA TCT GTT CAT CTG ACT CCT GCC ATC TCT GCT CCT AGT ATT GAC

Supplementary Table 2. The list of DNA substrates used to construct DNA chassis ([P]: phosphate, Cy3: Cyanine 3, Bio: biotin, AmMC6: Amino modifier C6).

Construct Name	Description	Vector	Source	Figures
SNAPf-Dyn	ZZ-Tev-SNAPf-DYNH1C1-IC2C-LIC2-Robl1-Tctex1-LC8	pOmniBac-pIDC	Schlager et al. 2014	F1c, F2a-c, F3,F5, F6, S1, S2, S3a-g, S4, S5f-h, S6
SNAPf-Dyn-Phi	ZZ-Tev-SNAPf-DYNH1C1$_{K1610/R1567E}$-IC2C-LIC2-Robl1-Tctex1-LC8	pOmniBac-pIDC	Zhang et al. 2017	F1d, F2d-g,, F4, F6, S3h, S7
BicD2N-GFP	ZZ-Tev-BicD2$^{1-400}$-GFP	pOmniBac	Schlager et al. 2014	F1, F2, F3, F4, S1,S2, S3, S4, S7
BicDR1-GFP	ZZ-Tev-BicDR1-GFP	pOmniBac	Urnavicius et al., 2018	F1, F2, F3, F4, S1,S2, S3, S4, S7
BicD2N-SNAPf	ZZ-Tev-BicD2$^{1-400}$-SNAPf	pOmniBac	Urnavicius et al., 2018	F5a,c, F6, S5f-h, S6
BicDR1-SNAPf	ZZ-Tev-BicDR1-SNAPf	pOmniBac	This study	F6, S4b-c
BicDR1$_{mut}$-GFP	ZZ-Tev-BicDR1$_{E165R/E167K}$-GFP	pOmniBac	This study	F4
SNAPf-Dyn$_{LT}$-GST	ZZ-Tev-SNAPf-DYNH1C1$^{1-1074}$-GST-IC2C-LIC2-Robl1-Tctex1-LC8	pOmniBac-pIDC	Urnavicius et al., 2018	F4, F5
SNAPf-Dyn$_{ST}$-GST	ZZ-Tev-SNAPf-DYNH1C1$^{1-481}$-GST	pOmniBac	This study	F4
K560-SNAPf-GFP	KIF5B$^{1-560}$-SNAPf-GFP-His6	pET21b	This study	F5b-c, F6, S4d-h

Supplementary Table 3. The list of constructs used in this study. A ZZ-Tev tag was inserted at the N-termini of dynein and cargo adaptor constructs for binding of protein to IgG beads, and the tag was cleaved by Tev protease to elute the protein from the beads. His6 tag was inserted at the C-terminus of kinesin for NiNTA affinity purification. The SNAPf tag was used to label the proteins with fluorescent dyes and biotin functionalized with benzyl guanine. A C-terminal GST tag was used to stabilize dimerization of dynein tail constructs (F: Figure, S: Supplementary Figure).

Supplementary Figures

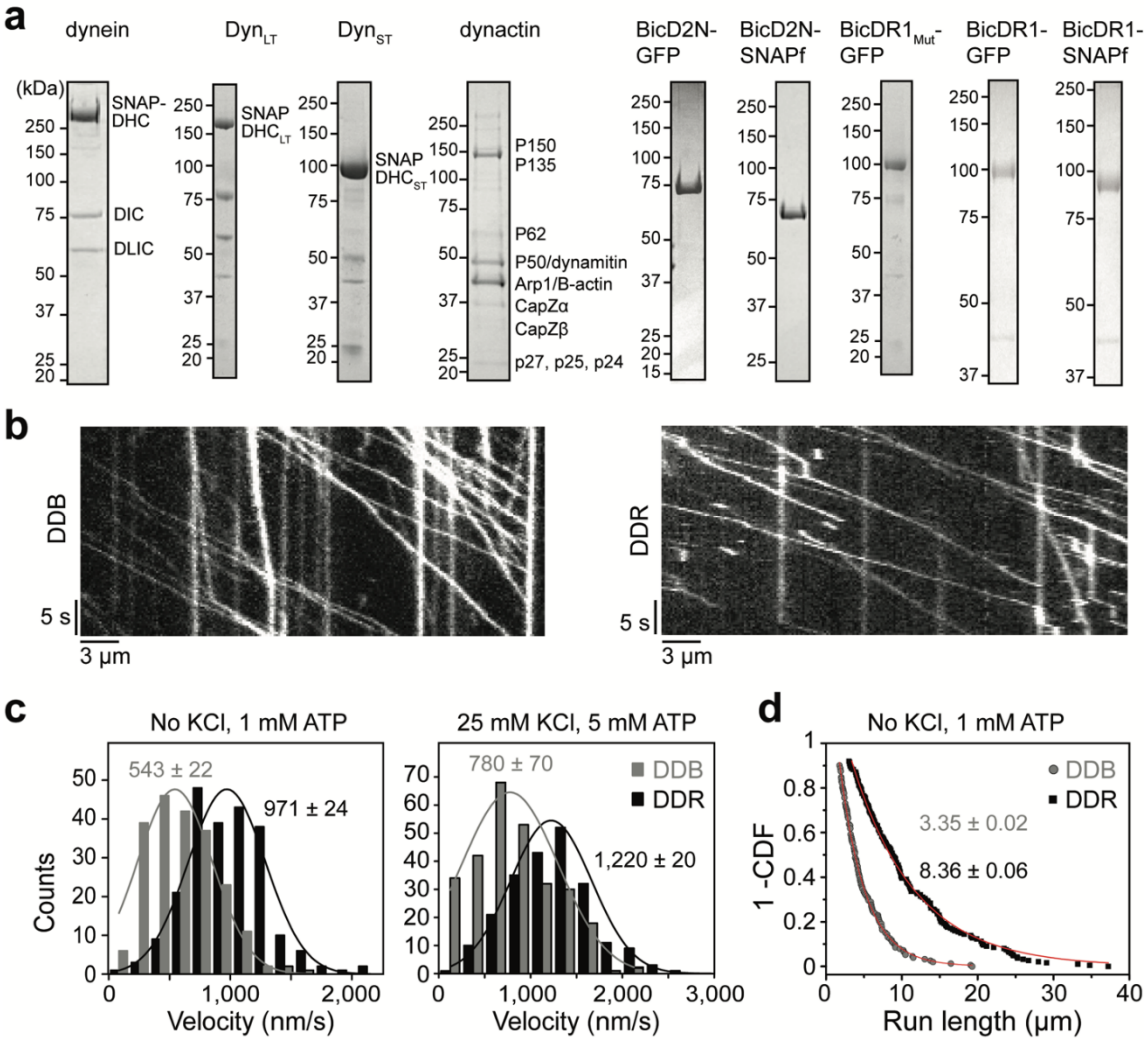

Supplementary figure 1. Purification and testing the motility of dynein/dynactin. (a) Denaturing agarose gels of purified dynein, dynactin and cargo adaptors. Bands corresponding to dynein and dynactin subunits are shown. Three independent protein preparations were used in the study. **(b)** Sample kymographs representing the motility of DDB and DDR in 25 mM KCl and 5 mM ATP. **(c)** Velocity histograms of DDB and DDR motility in 1 mM ATP and no salt (left) or in 5 mM ATP and 25 mM added KCl (right). Curves represent a fit to a Gaussian (mean ± s.e., n_{DDB} = 209, n_{DDR} = 223 on the left and n_{DDB} = 280, n_{DDR} = 219 on the right, three independent experiments per condition). Addition of salt and higher ATP resulted in faster motility of both DDR and DDB while the ratio of DDR to DDB velocity remained similar. **(d)** The inverse cumulative distribution function (CDF) for DDB and DDR run lengths along MTs. The red curves represent a fit to a single exponential decay to calculate the motor run length (decay rate ± s.e., n_{DDB} = 152, n_{DDR} = 187).

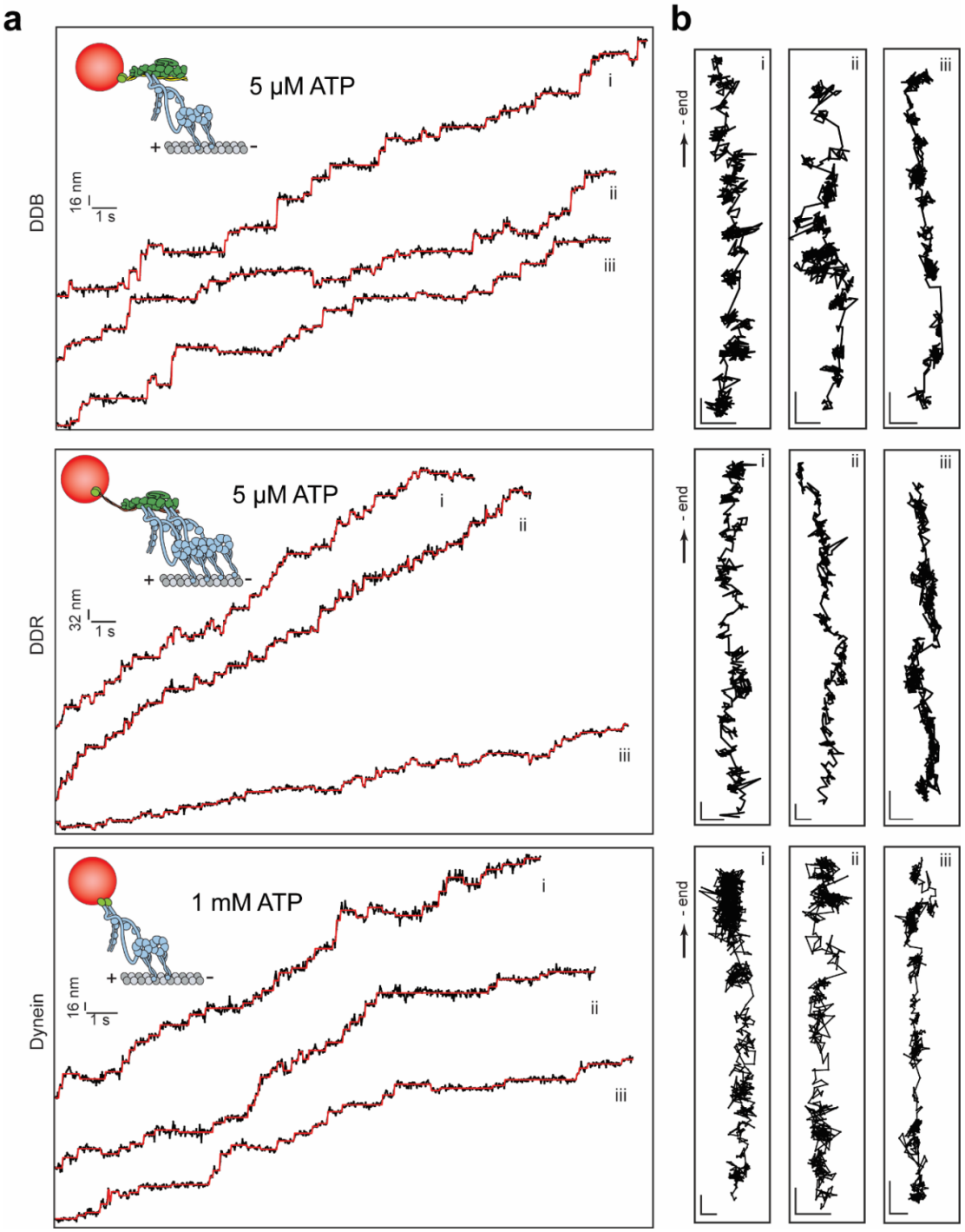

Supplementary figure 2. Example stepping trajectories of dynein, DDB, and DDR in the absence of load. (a) Additional three (i, ii and iii) examples of dynein, DDB, and DDR stepping along the MT long-axis. Horizontal lines represent a fit to a step finding algorithm. *n* = 21, 19 and 14 for longitudinal and 18, 19, and 14 for sideways traces of DDB, DDR, and dynein, respectively (10 independent experiments for each complex). **(b)** Two-dimensional representation of trajectories shown in a. Horizontal and vertical scale bars are 32 nm.

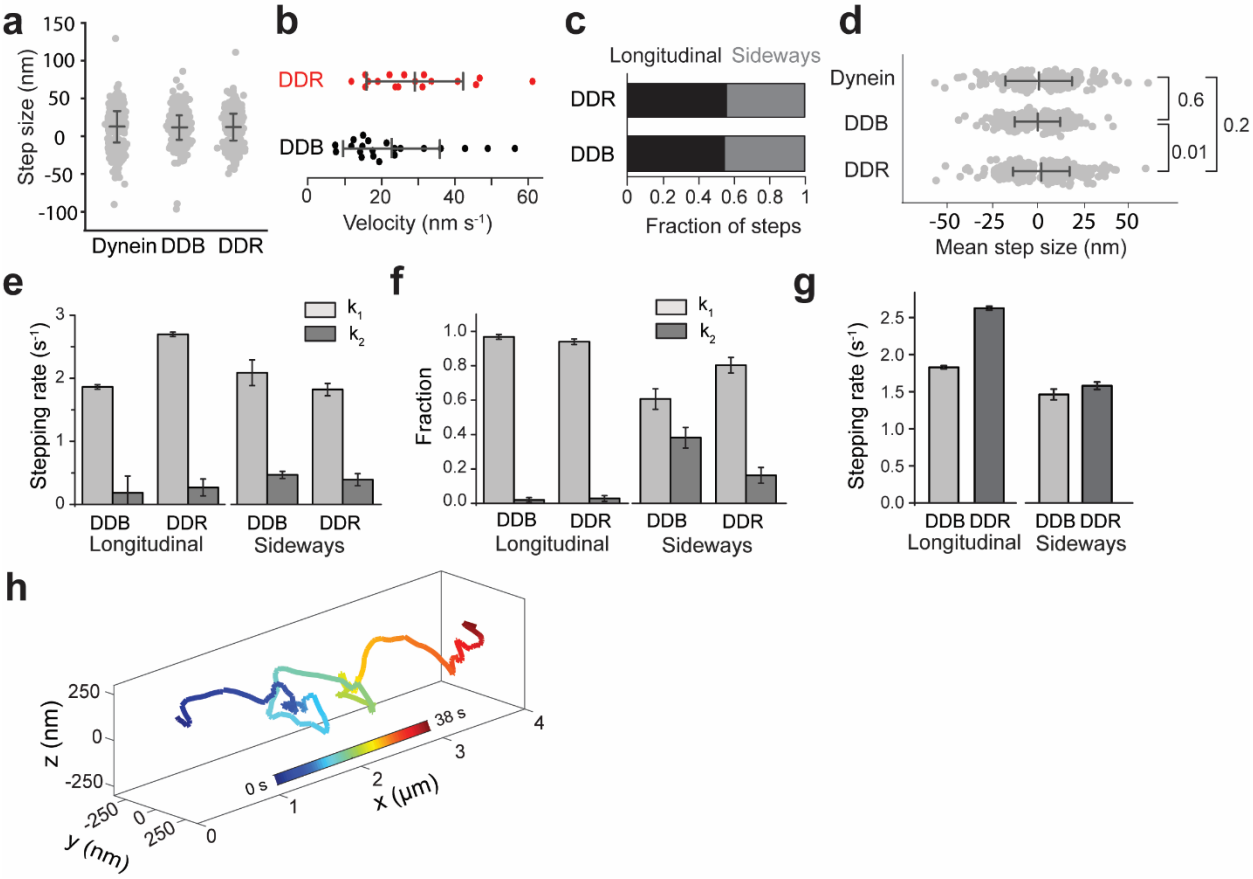

Supplementary figure 3. Stepping and dwell time analysis of dynein, DDB, and DDR in the absence of load. (a) Average step-size of dynein, DDB, and DDR along the MT long-axis (mean ± s.d., n = 715, 1061, and 963 steps, respectively). **(b)** Velocities of DDB and DDR traces included in step analysis (median ± 65% c.i., n = 21 and 17, respectively). **(c)** The fraction of longitudinal and sideways steps taken by DDB and DDR. **(d)** The average size of sideways steps taken by dynein, DDB, and DDR (mean ± s.d., n = 331, 463, and 534 steps, respectively). Positive and negative step size corresponds to rightward and leftward steps, respectively. p values are calculated using two-tailed t-test. **(e)** Stepping rates and **(f)** fractions of slow (k_1) and fast (k_2) longitudinal and sideways stepping (± 95% c.i.) estimated from the two-exponential fit in Figure 2c. In longitudinal stepping, both DDB and DDR mostly have the fast population, and DDR has higher k_1 and k_2 than DDB. In sideways stepping, although DDB has slightly higher k_1 and k_2 values than DDR, it has a higher fraction of slow population than DDR, resulting in slower sideways stepping of DDB compared to DDR. In e and f, n = 1430, 963 for longitudinal and 684, 534 for sideways stepping of DDB and DDR, respectively. **(g)** Weighted average of k_1 and k_2 for both longitudinal and sideways stepping (± 95% c.i.). **(h)** An example trajectory of a DDR-driven cargo bead that exhibits right-handed helical movement around the circumference of an MT (n = 16 beads from six independent experiments).

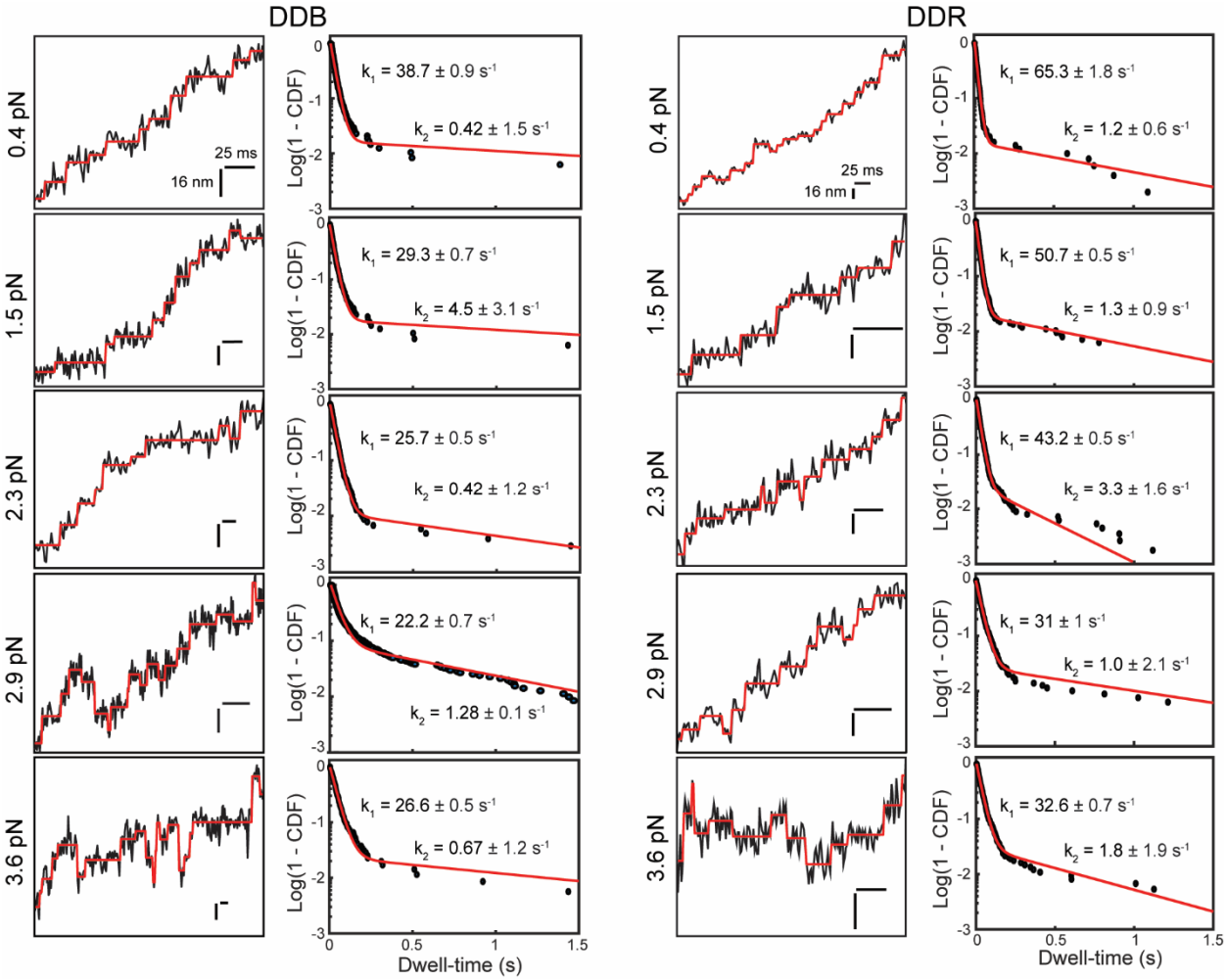

Supplementary figure 4. Stall force and dwell time analysis of DDB and DDR under load. (Left) Representative traces of beads driven by DDB and DDR under different hindering loads. (Right) The distribution of dwell times between consecutive steps was fitted to a two-exponential decay to calculate the fast (k_1) and slow (k_2) rate constants (mean ± s.e.). n = 480, 619, 1025, 709, and 352 dwells for DDB and 501, 1263, 1129, 792, and 741 dwells for DDR from 0.4 to 3.6 pN hindering load.

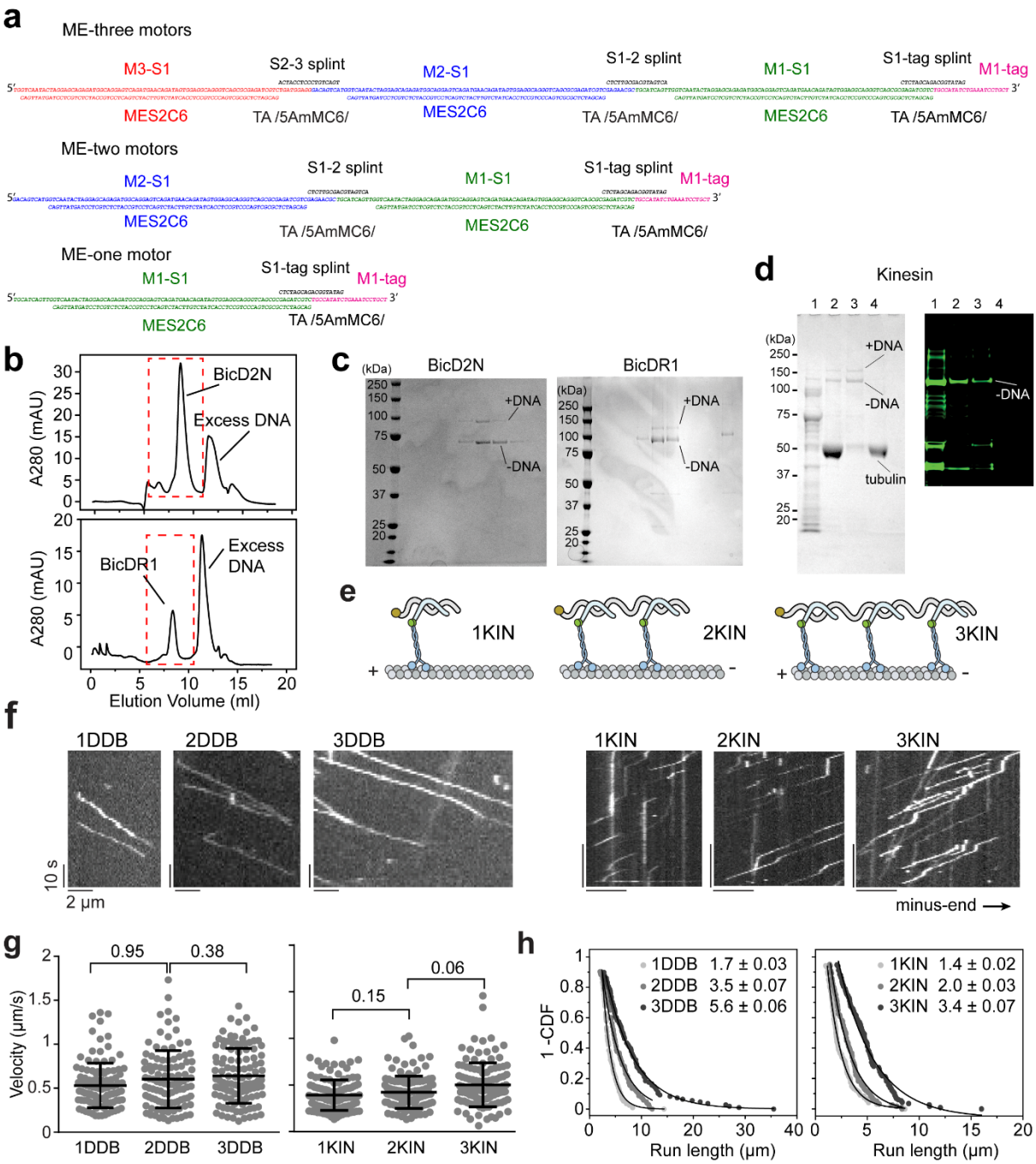

Supplementary figure 5. DNA chassis design for linking multiple motors. (a) DNA chassis were constructed by joining separate DNA fragments using short complementary DNA splints (black). The attachment sites were flanked with single-stranded DNA spacers to provide flexibility between multiple motors. The 3'-end of the chassis was labeled with Cy3 and biotin for fluorescence and optical trap assays, respectively. **(b)** BicD2N-SNAP and BicDR1-SNAP were sub-stoichiometrically labeled with a BG- functionalized DNA oligonucleotide. BicD2N and BicDR1 were separated from excess DNA through size exclusion. **(c)** A denaturing gel of the elutions from size exclusion (red dashed rectangles in

b) reveals DNA-labeled and unlabeled BicD2N and BicDR1 fractions. **(d)** Kinesin-SNAP was sub-stoichiometrically labeled with benzyl guanine (BG)-functionalized DNA oligonucleotide. Excess unreacted DNA was removed via the MT bind and release assay (1: kinesin sample, 2: kinesin pelleted with MTs, 3: kinesin released from MT and 4: pelleted MTs after kinesin release). The gel was imaged with Coomassie stain absorbance under brightfield (left) and TMR fluorescence under 532 nm excitation (right). In b-d, $n = 3$ independent experiments. **(e)** Schematic shows the assembly of multiple kinesins on DNA chassis. **(f)** Sample kymographs representing the motility of 1-3DDB and 1-3KIN chassis on MTs. **(g)** Velocities of DDB-and KIN-chassis on MTs The line and whiskers represent the mean and s.d., respectively. p values are calculated using two-tailed t-test. In f and g, $n = 115$, 103, 108, 120, 120, and 114 from left to right, three independent experiments per condition. **(h)** Inverse cumulative distributions of DDB- and KIN-chassis run lengths on MTs ($n = 115$, 103, 108, 120, 120, and 114 from left to right, three independent experiments per condition). Solid lines represent a fit to a single exponential decay (decay rate ± s.e.).

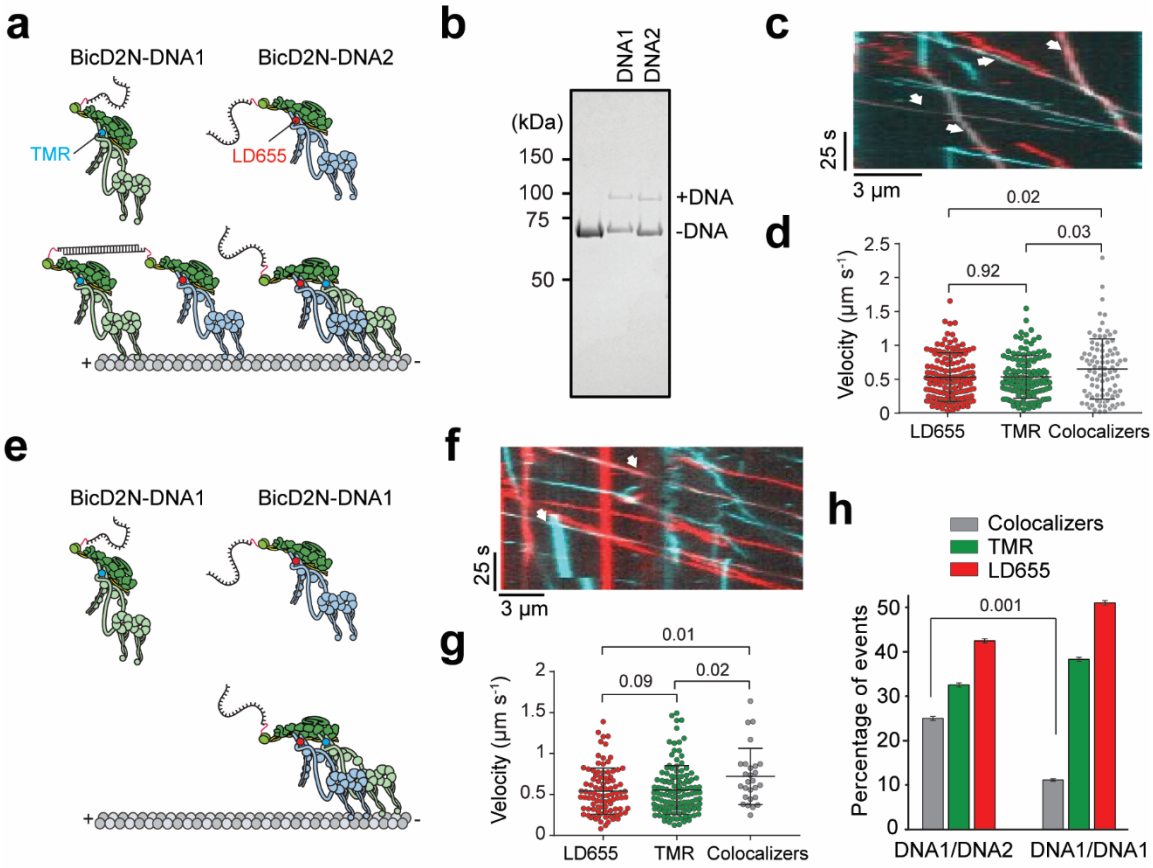

Supplementary figure 6. Linking two dyneins with complementary DNA oligos. (a) Strategy for linking two DDBs into a common DNA scaffold. TMR-LD655 colocalization can be observed either by the recruitment of two different-colored dyneins to a single BicD2N or by linking two DDBs to a common DNA scaffold through DNA hybridization. **(b)** BicD2N-SNAP was sub-stoichiometrically labeled with complementary DNA oligos (DNA1 and DNA2). DNA labeling efficiency was estimated from the denaturing gel. $n = 3$ independent experiments. **(c)** Sample kymograph shows the motility of TMR-dynein (cyan), LD655-dynein (red) and colocalization of TMR- and LD655-dyneins (white arrows). **(d)** Velocity distribution of TMR-dynein, LD655-dynein, and colocalizers (mean ± s.d.). In c and d, $n_{LD655} = 158$, $n_{TMR} = 121$, and $n_{colocalizers} = 93$, from three independent experiments. **(e)** Two different batches of BicD2N were labeled with the same DNA oligo. In this strategy, TMR-LD655 colocalization can only be observed by the recruitment of two different-colored dyneins to a single BicD2N, while colocalization through hybridization of two DDBs is eliminated. **(f)** Sample kymographs show the motility of TMR-dynein (cyan), LD655-dynein (red) or co-localizers (white arrows) when BicD2N were labeled with the same DNA oligo. **(g)** Velocity distribution of TMR-dynein, LD655-dynein, and colocalizers when BicD2N were labeled with the same DNA oligo (mean ± s.d.). **(h)** The percentage of TMR-dynein, LD655-dynein, and colocalizers that move processively along MTs. Errors are calculated

from multinomial distribution. p values are calculated using two proportions Z test. The percentage of co-localizing events was significantly higher when BicD2N were labeled with complementary oligos. In f-g, n_{LD655} = 124, n_{TMR} = 93, and $n_{colocalizers}$ = 29, from three independent experiments. In h, n = 352 for DNA1/DNA2 and 246 for DNA1/DNA1. In d and g, p values are calculated using two-tailed t-test.

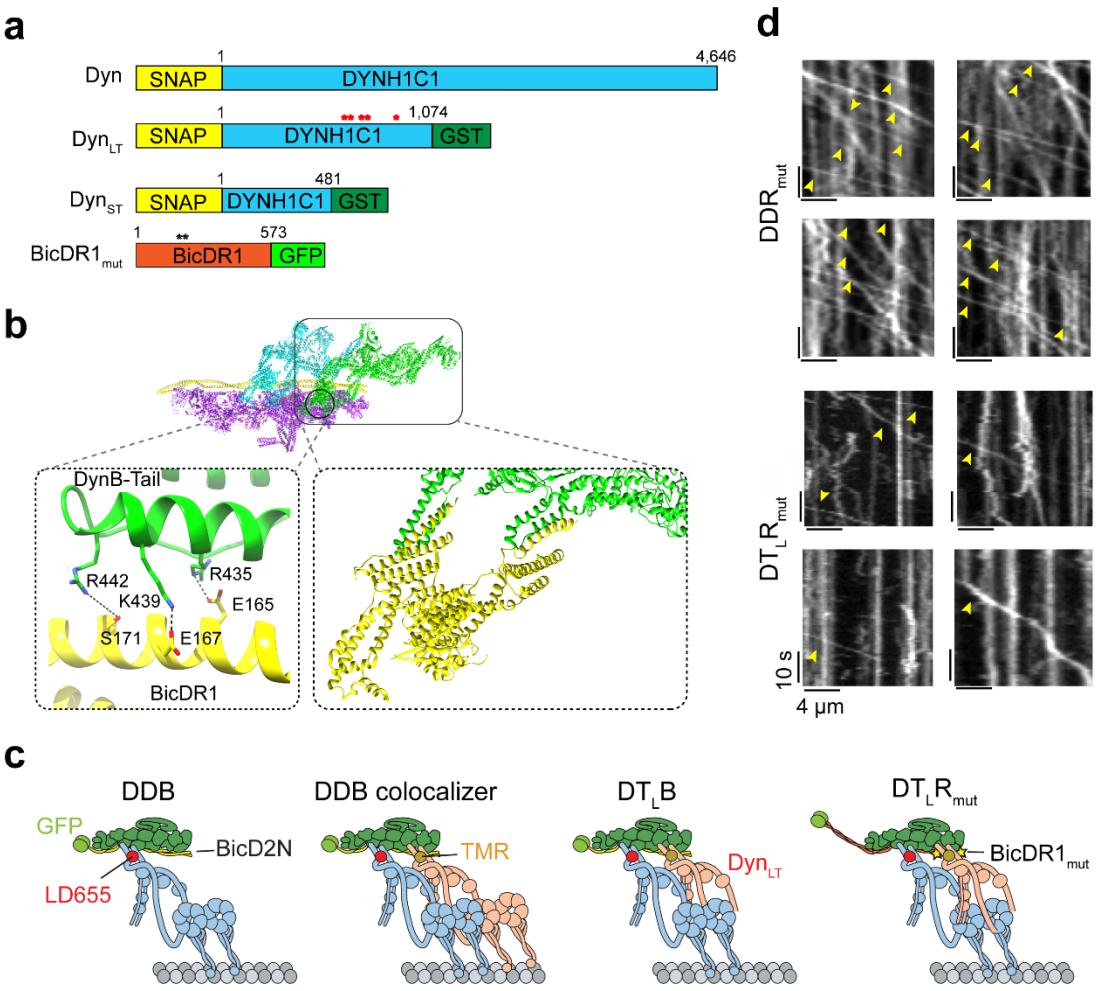

Supplementary figure 7. Engineering of mammalian dynein/dynactin. (a) Dynein was truncated at residues 1,047 and 481 to generate Dyn_{LT} and Dyn_{ST}, respectively. These constructs were tagged with a C-terminal GST to stabilize the dimer. Red stars show the location of tail-tail interaction sites identified by structural studies[30]. BicDR1 was mutated at the dynein B binding site (black stars). **(b)** (Top) Structure of DT_LR (PDB accession number: 6F1T) shows the interface between BicDR1 and dynein B chain B1. (Bottom left) Salt bridges between dynein B tail and BicDR1. E165R and E167K mutations were introduced to BicDR1 for a charge reversal. (Bottom right) Dyn_{ST} (yellow) is truncated after the N-terminal dimerization domain of DHC. This construct does not interact with light and intermediate light chains and is not expected to form extensive contacts with the other dynein recruited to dynactin. **(c)** Schematics represent the configuration of different DDB and DDR assemblies with full-length and truncated dynein constructs labeled with different dyes. **(d)** Representative kymographs of LD655-dynein (yellow arrowheads) in the presence of dynactin and $BicDR1_{mut}$ (DDR_{mut}) and in the presence of dynactin, $BicDR1_{mut}$, and Dyn_{LT} (DT_LR_{mut}) from three independent experiments.

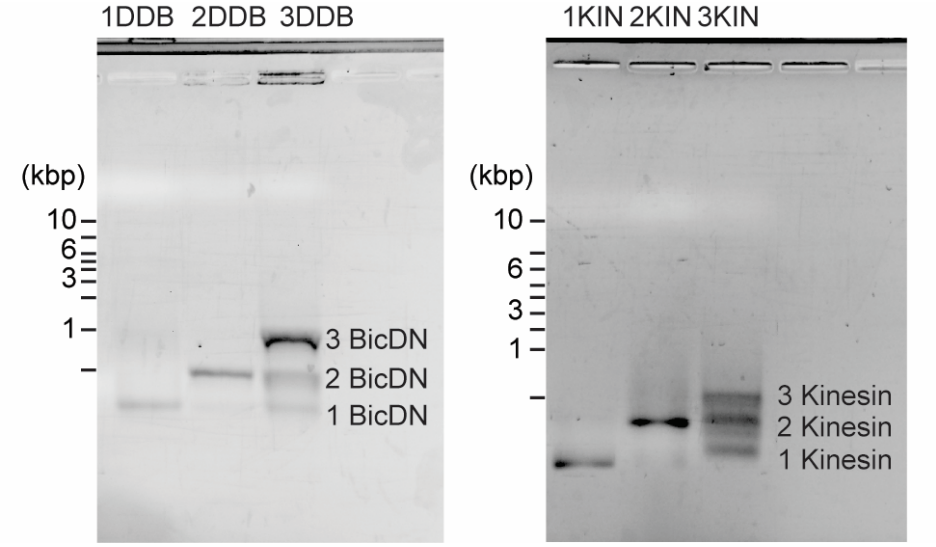

Supplementary figure 8. Full images of the native agarose gel in Figure 5d. The agarose gel shows the quantification of DNA chassis labeled with 1, 2, and 3 BicD2Ns (left) or kinesin-1 motors (right).

Supplementary Video Legends:

Supplementary Video 1. Processive motility of single DDB and DDR complexes along MTs in 1 mM ATP. Dynein was labeled with TMR and imaged under TIRF illumination. Stopwatch shows time in seconds. Scale bars are 5 μm. Three independent experiments were performed for each condition.

Supplementary Video 2. Helical movement of DDB- and DDR-driven beads along an MT bridge. 0.5 μm diameter beads were coated with multiple DDBs or DDRs and brought near an MT bridge. After the bead attaches to an MT, it was released from the trap and its helical motility around the circumference of an MT bridge was tracked in three dimensions. The assays were performed in the presence of 1 mM ATP. The samples were imaged under brightfield illumination. Stopwatch shows time in seconds. Scale bar is 1 μm. Eleven and six independent experiments were performed for DDB and DDR, respectively.

Supplementary Video 3. Linking of two DDBs via DNA hybridization. (Top) BicD2N was labeled with complementary DNA oligonucleotides (DNA1 and DNA2). BicD2N-DNA1 was mixed with TMR-dynein (cyan) and dynactin, and BicD2N-DNA2 was mixed with LD655-dynein (red) and dynactin to assemble DDB. Two DDB assemblies were connected through DNA hybridization. (Bottom) The BicD2N subunits of two DDB assemblies were labeled with the same oligonucleotide to prevent colocalization through DNA hybridization. In this assay, colocalization occurs through recruitment of two dyneins to dynactin by BicD2N. Dynein/dynactin motility along surface-immobilized MTs was recorded in 1 mM ATP with two-color TIRF illumination. Colocalizers are marked with white arrows. Stopwatch shows time in seconds. Scale bars are 5 μm. Three independent experiments were performed for each condition.

Supplementary Video 4. Motility of DDB-kinesin and DDR-kinesin colocalizers. Two-color TIRF imaging of TMR-kinesin (cyan) and LD655-dynein (red) motility along MTs in 1 mM ATP. Colocalizers are marked with white arrows. Stopwatch shows time in seconds. Scale bars are 5 μm. Three independent experiments were performed for each condition.